ENHANCING POWER QUALITY IN EV CHARGING STATIONS: THE ROLE OF FAULT RIDE THROUGH DURING VOLTAGE DISTURBANCES

B. Sruthi, UG Student, Sree Vahini Institute of Science and Technology (Autonomous), Tiruvuru, Andhra Pradesh
N. Lohitha, UG Student, Sree Vahini Institute of Science and Technology (Autonomous), Tiruvuru, Andhra Pradesh
M. Surendra, UG Student, Sree Vahini Institute of Science and Technology (Autonomous), Tiruvuru, Andhra Pradesh
S. Vasanth, UG Student, Sree Vahini Institute of Science and Technology (Autonomous), Tiruvuru, Andhra Pradesh
Dr Kiran Kumar K Assoc. Professor, Dept of EEE, Sree Vahini Institute of Science & Technology (Autonomous), Tiruvuru.

Abstract:
The successful operation of the electric vehicle (EV) charging system depends on a high-quality power source. Nonetheless, one of the primary issues with the distribution system is the quality of the power. In order to improve the voltage quality, this paper offers a fault ride-through capability (FRTC) and focuses at how voltage disturbance affects EV batteries and charging systems. The dc–dc converter and the three-phase regulated rectifier constitute the charging system. Lithium-ion batteries are used for imitating the EV battery pack. The dynamic voltage restorer is the means by which the FRTC system achieves its objective of improving voltage quality. It protects the charging system and EV batteries from hazardous high voltage sag levels. The MATLAB/Simulink platform is being used to analyze the performance of the proposed EV charging station (EVCS) in 30%, 60%, and 90% voltage sag. Additionally, the software-in-the-loop test is being used to do the real-time validation with the assistance of the dSPACE (DS1202) real-time system. The performance of the FRTC-equipped EVCS is superior than that of the traditional EVCS.

Index Terms:
power quality, fault ride-through capability (FRTC), electric vehicle (EV) chargers, distribution grid and voltage sag.

I. INTRODUCTION

Future power grids will undoubtedly have to handle the strain of electric cars (EVs). In terms of power consumption, voltage imbalances, stability, harmonic pollution, and other adverse effects, the distribution grid's large-scale integration of EV charging stations (EVCSs) having an influence on power quality [1], [2]. Additionally, for the EV charging system to function properly, a high-quality power source is needed. In reality, though, there are a number of power quality problems with the grid supply. Because of abrupt changes in load, electric motor starting, distribution grid faults, power line accidents and transformer energization, voltage quality is the main problem in the distribution grid [3], [4].

The EV charging profile and battery life cycle are directly impacted by poor power quality. The effect of EV charging on the distribution grid is being the focus of extensive investigation in recent years. In [5], the effects of plug-in electric vehicles on the distribution power system have been examined. [6] reviews the power converter topologies, battery charging control techniques, and different effects of the EV loads on the low-voltage distribution grid, including harmonics, voltage quality, imbalances, and feeder problems. In [7], the effects of EVs on the economy, ecology, power grid, and different charging standards are covered. In [8], the effects of plug-in hybrid EVs on aging, distribution transformer overload and voltage quality are evaluated.

The effects of grid disruptions on the EV charging infrastructure, however, received less attention in the studies. Furthermore, the behavior of chargers during grid disruptions is not addressed by a standard (J2894) created by the Society of Automotive Engineers (SAE) for plug-in EVs [9]. As a

 ISSN: 2278-4632
Vol-15, Issue-04, No.02, April: 2025

result, precise analysis is needed to supply the EV charging system with a high-quality power source. A small number of studies evaluated if grid voltage sag affected EV batteries. The crucial value is established in [10] after an investigation of the impact of voltage sag on EV chargers. The PWM converter-based EV charger critical voltage sag is established by the small-signal stability study. It is readily evident that even after the voltage sag is compensated for, the EV charging system abruptly collapses during deep voltage sag and is unable to return to its typical operational state. In grid-to-vehicle, vehicle-to-home, and vehicle-to-grid operations, the effects of many real-world scenarios of voltage sag, load fluctuation, and voltage imbalance on EV chargers have been examined. According to the results in [11], the battery current has been adjusted in response to variations in load in the vehicle-to-home mode and the three-phase voltage imbalances and voltage sag have an impact on the EV charging profile in the grid-to-vehicle mode. In [12], the effects of single-, two-, and three-phase voltage sag on chargers based on PWM converters, six, 12 and three-pulses are also examined. EV chargers and batteries are more affected by the three-phase critical voltage sag. Additionally, 50% of the cost of an EV is related to its battery [13]. Therefore, in order safeguard the batteries and charging system from the critical voltage sag circumstances, the voltage quality enhancement approach is necessary.

The fault ride-through capability (FRTC) system is suggested in a variety of publications to improve the voltage quality for a range of applications, including hybrid energy storage systems in the distribution grid, wind and solar. The dynamic voltage restorer (DVR), static VAR compensator, crowbar and fault current limiter (FCL) are typically used to accomplish FRTC. A DVR is being used in [10] to improve the voltage quality and reduce the sensitive load's phase jump problems. Voltage sag effects on changeable speed drives are examined in the study [15], and the improved synchronous reference frame (SRF) theory-based DVR enables to reduce it. In order to improve the FRTC of the wind energy conversion system based on doubly fed induction generators, the DVR is employed in [12]. The distribution grid's transient voltage is controlled by the superconducting FCL and superconducting magnetic energy storage-based DVR. The results achieved are contrasted with the crowbar technique and the distribution static compensator. The DVR-FRTC system performs best for improving voltage quality among these methods. For EVCS, the DVR-FRTC system is recommended. Additionally, this article's primary contributions are listed below.

1) The effects of voltage sag on batteries and EV charging systems are being studied.
2) The FRTC system based on DVR is intended for EVCS.
3) It offers an alternative to lessen the effects of grid voltage sag on batteries and EV charging infrastructure.
4) It prevents against significant voltage sag in the batteries and EV charging system.
5) Despite the crucial voltage sag occurring at the distribution grid, it maintains the charging system in stable mode by controlling the load voltage.

II. PROPOSED EVCS MODEL

The proposed FRTC integrated EVCS concept is shown in Fig. 1. A DVR-based FRTC system, a chopper and a regulated rectifier compose this setup. The grid ac power is transformed into a predetermined dc power by the regulated rectifier. The constant dc supply is converted into the proper voltage and current for battery charging by the dc–dc converter. Through the injection transformer, the DVR is linked to the grid. In the event of grid supply disruptions, the DVR-FRTC system is utilized to improve the quality of the load voltage. Models of EV battery packs use lithium-ion batteries. Fig. 2 shows a comprehensive circuit schematic of the proposed EVCS.

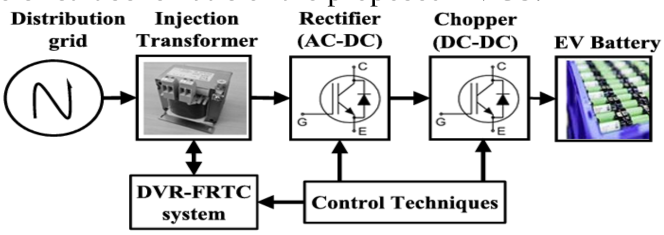

Fig. 1. Schematic of the proposed EVCS.

 ISSN: 2278-4632
Vol-15, Issue-04, No.02, April: 2025

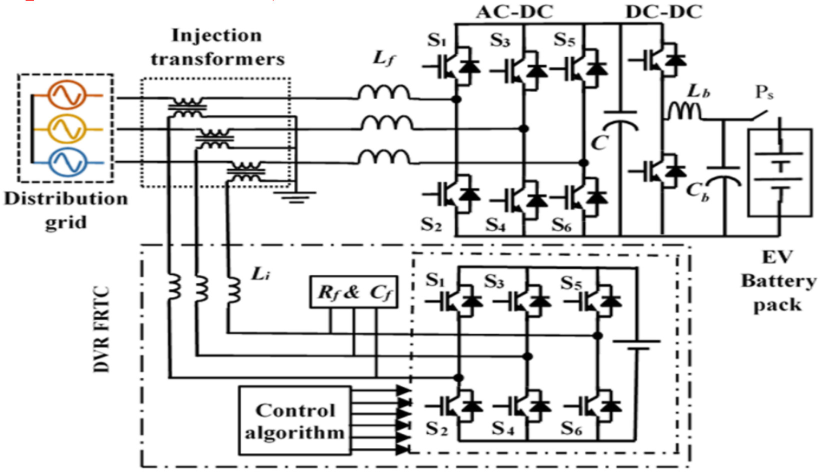

Fig. 2. Circuit diagram of the proposed EVCS.

Electric vehicle charger design:

The chopper and controlled rectifier are the two components that comprise up the EV charger. At the inductive filter, the utility grid is connected to the rectifier input. In order to avoid unnecessary switching losses, the rectifier output voltage should be low enough and high enough to offer effective dynamic control. The following calculation is used to measure the dc voltage:

$$V_{dc} = \frac{2\sqrt{2}V_{L-L}}{\sqrt{3}m} \qquad (1)$$

where VL−L is the line voltage and m are the modulation index. To prevent the overmodulation effect, m is adjusted to 0.9 and the VL−L is set to be 415 V. Vdc is therefore determined to be 752 V and selected to be 750 V. The waves in the rectifier output voltage are eliminated by the filter capacitor (C). The following formula determines the filter capacitor's necessary value.

$$C = \frac{P_{dc}}{V_{dc} \times 4\pi \times f \times \Delta V_{dc}} \qquad (2)$$

where Pdc is the rated dc power (14 kW), Vdc is the ripple voltage and f is the grid frequency (50 Hz). Vdc is equivalent to 1.5% of the output voltage of the rectifier. C is consequently determined to be 2862 µF and chosen to be 3300 µF.

The battery is connected to the rectifier output terminals via a chopper. It provides the proper voltage and current for battery charging and controls the rectifier output voltage. The following formulas [26] are used to calculate the chopper inductor (Lb) and capacitor (Cb):

$$L_b = \frac{D(V_{dc} - V_b)}{f_s \times \Delta I_L} \qquad (3)$$

$$C_b = \frac{\Delta I_L}{8 \times f_s \times \Delta V_b} \qquad (4)$$

where Vb is the output ripple voltage, D is the duty ratio and Vb is the battery voltage. The switching frequency is fs, and the ripple current is denoted by IL.

Lithium-Ion Battery Architecture:

High energy density and specific power are two other benefits of the lithium-ion battery. It is hence more favored for EV applications. The battery charging (5) and discharging (6) dynamic equations are given below [26]:

$$V_{nl} = V_o - R_i i - K\frac{Q}{q + 0.1Q}i^* - K\frac{Q}{Q - q}q + Ae^{-Bq} \qquad (5)$$

$$V_{nl} = V_o - R_i i - K\frac{Q}{Q - q}i^* - K\frac{Q}{Q - q}q + Ae^{-Bq} \qquad (6)$$

where A is the exponential voltage (V), B is the exponential capacity (Ah−1), Q is the maximum battery capacity (Ah), i is the battery current (A), i∗ is the low-frequency current dynamics (A), Vo is the battery nominal voltage (V), q is the extracted capacity (Ah), A is the exponential voltage (V) and K is the polarization constant (Ah−1). The state of charge (SOC) of the battery is determined by

$$SOC = \left(1 - \frac{1}{Q}\int_0^t i\,(t)dt\right) \times 100 \qquad (7)$$

The battery is said to be empty when its state of charge (SOC) is 0%, and full when it is 100%.

DVR-Based FRTC System Construction:

A three-phase voltage-source converter, an injection transformer, an auxiliary inductor, a ripple filter and a dc voltage source comprise the majority of the DVR-based FRTC system. The voltage-source converter and injection transformer of the DVR power rating (VA) is determined by (8). In [27]

$$S_{DVR} = 3 \times V_{vsc} \times I_{vsc} \qquad (8)$$

where Vvsc and Ivsc stand for the voltage-source converter voltage and current ratings, respectively. The following formula can be used to get Vvsc for the unity power factor load:

$$V_{VSC} = \sqrt{V_r^2 - V_a^2} \qquad (9)$$

where Va is the actual source voltage during sag and Vr is the rated source voltage. Based on the DVR ripple current, the interface inductor (Li) for the voltage-source converter is calculated and represented as follows:

$$L_i = t_r \times 0.866 \times m_D \times V_{Ddc}/(6 \times a \times f_{Ds} \times \Delta I_r \qquad (10)$$

where Ir is the ripple current, af is the overloading factor, fDs is the DVR switching frequency, VDdc is the DVR dc-link voltage, mD is the DVR modulation index, and tr is the injection transformer turns ratio. The DVR's ripple filter may be approximated by

$$f_{RF} = 1/(2 \times \pi \times R_f \times C_f \qquad (11)$$

where the ripple filter frequency is denoted by fRF, the resistance by Rf, and the capacitance by Cf.

III. Techniques for control

The converters utilized in the DVR-FRTC integrated EVCS must operate properly, which requires effective control strategies. In [28]– [30], a variety of control methods are being introduced for the rectifier, including voltage-oriented control, direct power control (DPC), and virtual flux DPC (VFDPC) methodology. In DPC and VFDPC approaches, the variable switching frequency is employed. It requires for a high-speed processor and complicates the filter design. The VOC approach, on the various present, uses a set switching frequency. Consequently, it lessens the complexity of filter design. Additionally, it offers superior static performance and a quicker dynamic reaction by the inner current control loop. Consequently, the VOC approach is used for the rectifier in this study. In Fig. 3, the rectifier control approach (VOC) is displayed. With this approach, the inner loop regulates the current while the outer loop regulates the voltage. Using the following formula, the current and voltage "abc" coordinates are converted to "dq0" coordinates:

$$\begin{bmatrix} V_d \\ V_q \\ V_0 \end{bmatrix} = \frac{2}{3}\begin{bmatrix} \sin(\omega t) & \sin(\omega t - \frac{2\pi}{3}) & \sin(\omega t + \frac{2\pi}{3}) \\ \cos(\omega t) & \cos(\omega t - \frac{2\pi}{3}) & \cos(\omega t + \frac{2\pi}{3}) \\ \frac{1}{2} & \frac{1}{2} & \frac{1}{2} \end{bmatrix} \times \begin{bmatrix} V_a \\ V_b \\ V_c \end{bmatrix} \qquad (12)$$

The referenced-axis current is determined as (13), with the reference q-axis current being zero, using the error of the output dc voltage as input through the PI controller.

$$I_d^* = K_p(V_{dc}^* - V_{dc}) + \int K_i(V_{dc}^* - V_{dc}) \qquad (13)$$

The following equation is used to determine the reference "dq0" coordinate voltages:

$$V_d^* = V_d - K_p(I_d^* - I_d) - \int K_i(I_d^* - I_d) + \omega L I_q \qquad (14)$$

$$V_q^* = V_q - K_p(I_q^* - I_q) - \int K_i(I_q^* - I_q) - \omega L I_d \qquad (15)$$

ISSN: 2278-4632
Vol-15, Issue-04, No.02, April: 2025

The reference "dq0" coordinate voltages are then converted into "abc" coordinates by (16), and the resulting voltages are delivered to the PWM generator to produce the rectifier switches gating pulses.

$$\begin{bmatrix} V_a \\ V_b \\ V_c \end{bmatrix} = \begin{bmatrix} \sin(\omega t) & \cos(\omega t) & 1 \\ \sin(\omega t - \frac{2\pi}{3}) & \cos(\omega t - \frac{2\pi}{3}) & 1 \\ \sin(\omega t + \frac{2\pi}{3}) & \cos(\omega t + \frac{2\pi}{3}) & 1 \end{bmatrix} \times \begin{bmatrix} V_d \\ V_q \\ V_0 \end{bmatrix} \qquad (16)$$

The phase-locked loop (PLL) system computes the angular position (ωt).

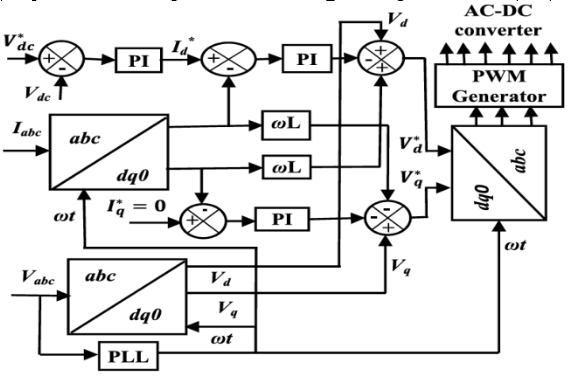

Fig. 3. Rectifier control strategy.

The battery charging techniques are used to determine the chopper control mechanism. The many battery charging techniques include taper and float charge, constant power (CP), constant voltage (CV), trickle current (TC), constant current (CC), and CCCV charging [7], [31]. The battery is overcharged while using the CC technique, and it takes longer to charge when using the CV approach. The battery with a lower current value is charged by TC charging. Lead-acid batteries are suitable for float charging. The CCCV approach, on the other hand, is mostly utilized for EV applications as it charges the battery by CC until the SOC reaches 80% and switches to CV mode at that point. Thus, the CV charges the remaining 20% SOC. CV charging in CCCV is three times slower than CC charging, which directly affects charging efficiency. The chopper uses a multistep CC approach to get around this restriction. Fig. 4 shows the chopper control method.

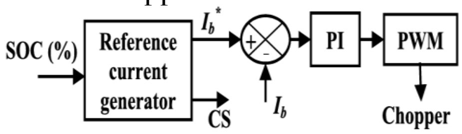

Fig.4. Control technique of the chopper.

The DVR-FRTC system's control algorithm is its most crucial component as the reference signal generating technique determines the DVR performance. Many time and frequency-domain control algorithms exist, including the neural network, the adaptive detecting theory, the PQ theory, the unit template theory, the single-phase DQ theory, the Kalman filter, the wavelet transform and the discrete Fourier transform, respectively [27]. Power quality is monitored using frequency-domain techniques, while the DVR is controlled using time-domain approaches. Among these methods, the control algorithm based on SRF theory is frequently employed to regulate the DVR [32]. For the DVR-FRTC system, the SRF control algorithm is thus used. Fig. 5 shows the SRF control algorithm in operation.

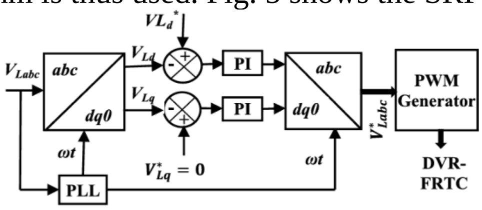

Fig.5. Control technique of the DVR-FRTC system.

The equation (12) is used to translate the "abc" coordinates of the load voltages (VLabc) into "dqo" coordinates (VLd, VLq). The PI controllers limit the voltage errors after comparing the converted voltages to reference voltages (V∗ Ld, V∗ Lq). (16) is used to translate the regulated voltages from

 ISSN: 2278-4632
Vol-15, Issue-04, No.02, April: 2025

"dq0" coordinates to "abc" coordinates. These "abc" coordinate voltages (V∗ Labc) are utilized in the PWM to produce the DVR-FRTC system switching signals.

IV. SIMULATION RESULTS

The MATLAB/Simulink platform is used to model the proposed DVR-FRTC integrated EVCS. For several sag levels, such as 30%, 60%, and 90%, the EVCS performance is examined both with and without DVR-FRTC. Table II lists the simulation settings that were applied to the system being modeled. For evaluating the effectiveness of the suggested system, a number of parameters are tracked, including grid voltage, load voltage, injecting voltage, output dc voltage, battery charging current, battery voltage and battery state of charge.

Table II System Details

Parameters	Symbol	Values
Grid voltage	V_s	415V (ph-ph)
Grid frequency	f	50Hz
Filter inductor	L_f	5mH
Filter capacitor	C	3300μF
DC output voltage	V_{dc}	750V
Chopper capacitor	C_b	50μF
Chopper inductor	L_b	4mH
Battery nominal voltage	V_0	360V
Battery capacity	Q	66.2Ah
Switching frequency	f_s	10KHz
Interfacing inductor	L_i	3mH
Ripple filter	R_f, C_f	5Ω, 30μF

Analysis of Performance Without DVR-FRTC

The EVCS performance without DVR-FRTC is evaluated for sags of 30%, 60% and 90%, respectively. Fig. 6 shows the performance parameters at 30% sag. The grid voltage sags by 30% between 0.15 and 0.25 seconds. Because the DVR-FRTC system is not there, the injecting voltage is zero. As a result, the load voltage experiences the same sag. Nevertheless, the rectifier generates the output dc voltage that is predetermined. As a result, the system is run in a stable manner. Fig. 7 shows the equivalent battery properties.

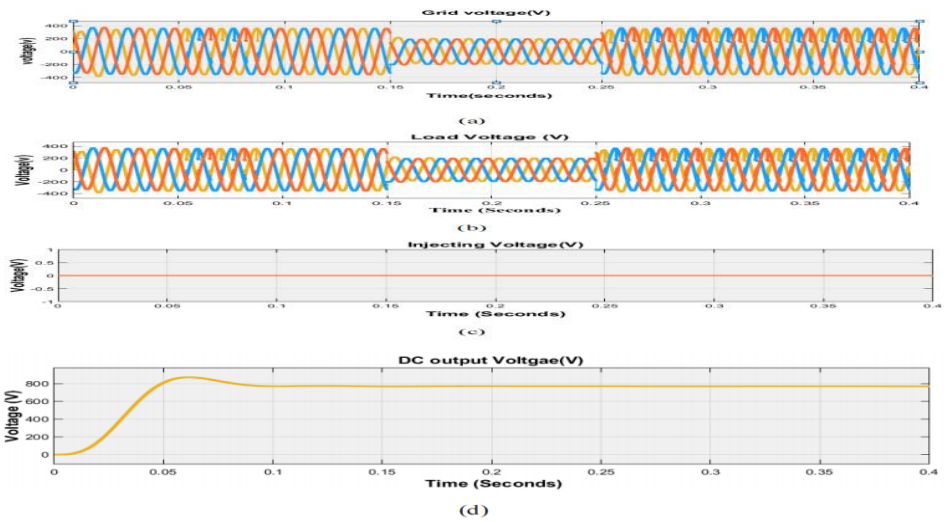

Fig. 6. Performance characteristics without FRTC at 30% sag.

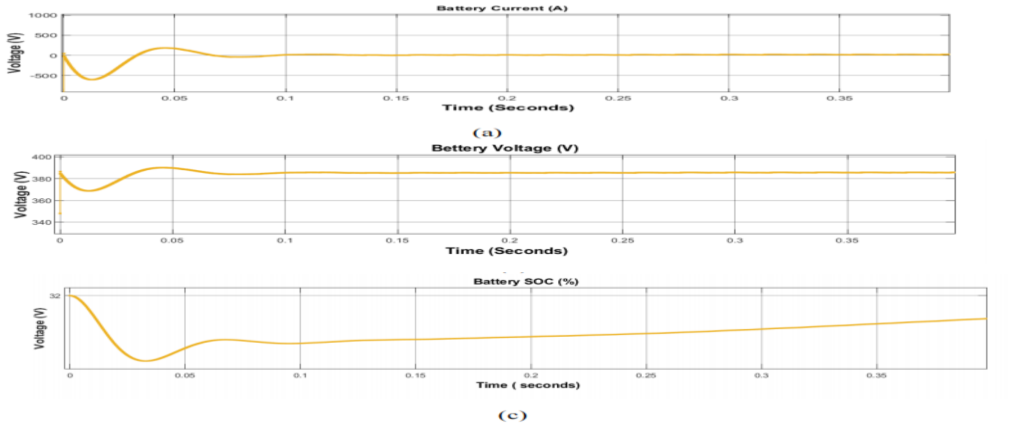

Fig. 7. Battery characteristics without FRTC at 30% sag.

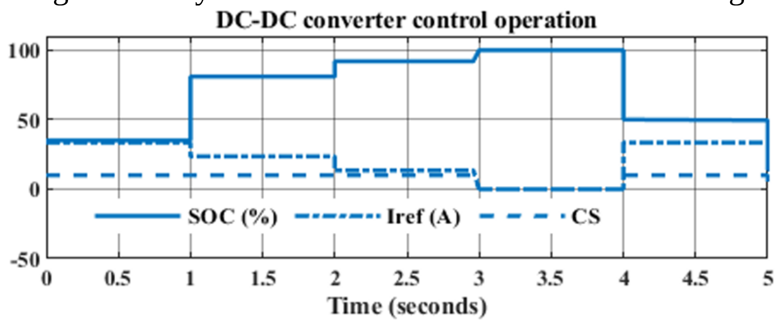

Fig. 8. Performance of the chopper control technique.

Investigation with DVR- Performance FRTC 30 %

The effectiveness of the EVCS with DVR-FRTC is examined for a range of voltage sag levels, including 30%, 60% and 90%, in that order. Fig. 13 shows the performance parameters of 30% sag. At 0.15 seconds, the grid voltage experiences a sag. The DVR-FRTC system applies the voltage to the load during this time. As a result, the load voltage is kept at its typical level. Additionally, the rectifier generated the desired dc output voltage. As a result, the system is run in a stable manner. Fig. 14 shows the battery characteristics for this operation mode.

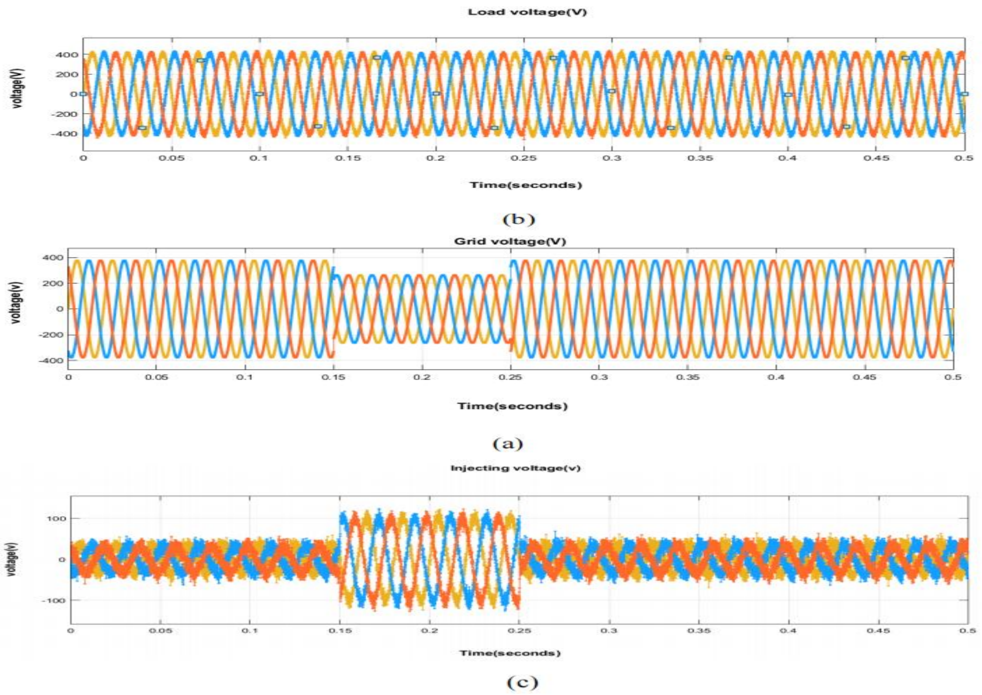

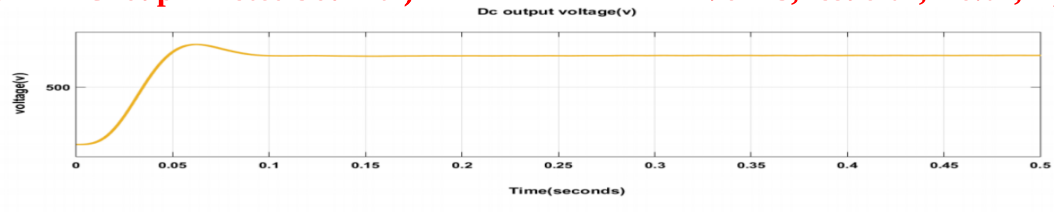

(d)

Fig. 13. Performance characteristics with FRTC at 30% sag.

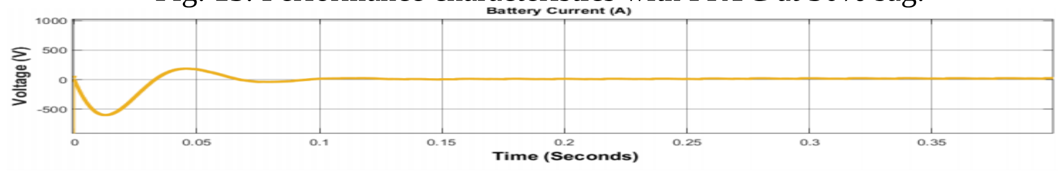

(a)

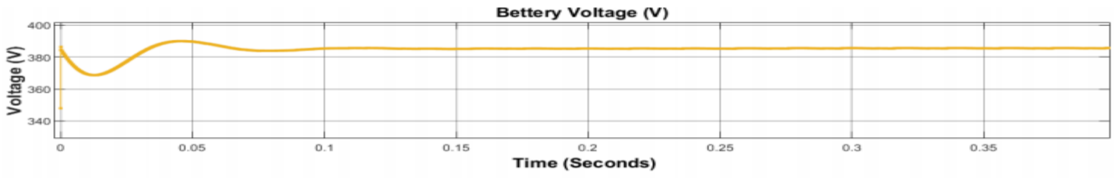

(b)

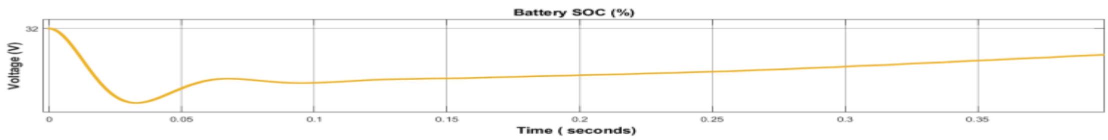

(c)

Fig. 14. Battery characteristics with FRTC at 30% sag.

Fig. 15 shows the DVR-FRTC system performance parameters during the 60% voltage sag. The DVR-FRTC begins injecting the voltage in phase with the load voltage during the voltage sag interval. As a result, the system maintains a stable performing state by regulating the load voltage to its rated value. Additionally, a nominal value for the rectifier output voltage is maintained. Even when 60% voltage sag occurs, the battery current, voltage, and state of charge remain at a nominal level, as seen in Fig. 16.

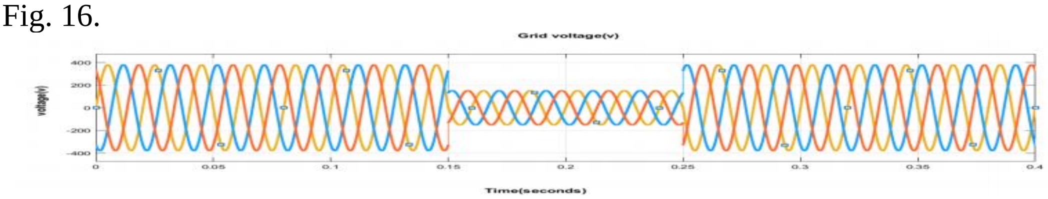

(a)

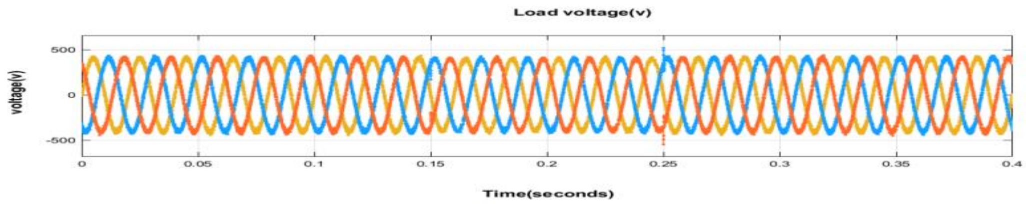

(b)

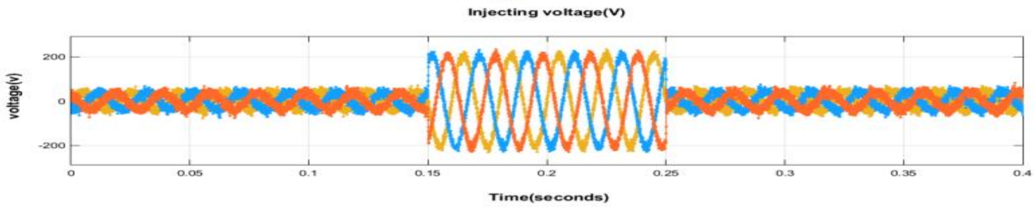

(c)

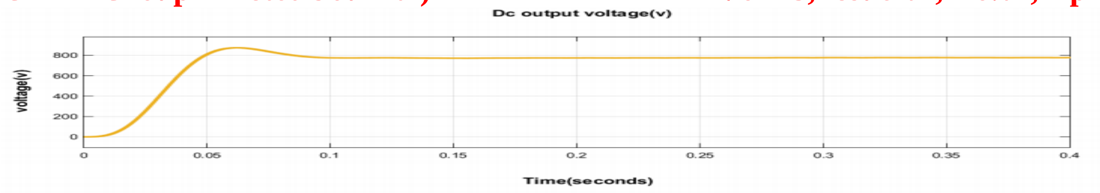

(d)

Fig. 15. Performance characteristics with FRTC at 60% sag.

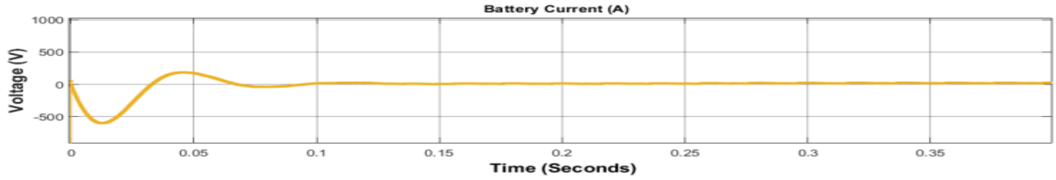

(a)

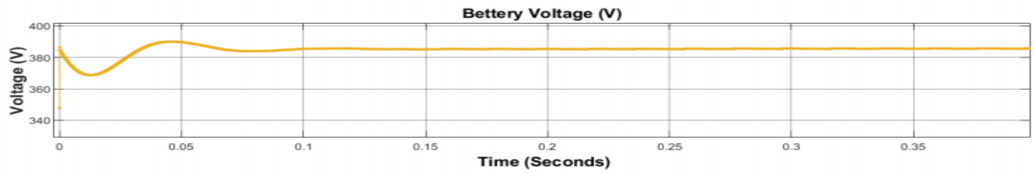

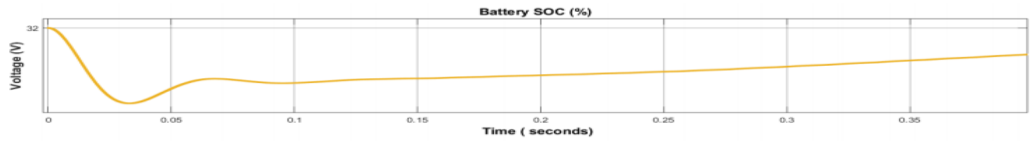

(C)

Fig. 16. Battery characteristics with FRTC at 60% sag.

The EVCS performance parameters with FRTC at 90% voltage sag are displayed in Fig. 17. In this case, the load voltage adheres to the norm. When the voltage is injected by the DVR-FRTC system when voltage sag occurs. As a result, the predetermined value of the dc output voltage is maintained. It maintains the proper level of battery voltage, current and state of charge. Fig. 18 presents the battery characteristics for this mode.

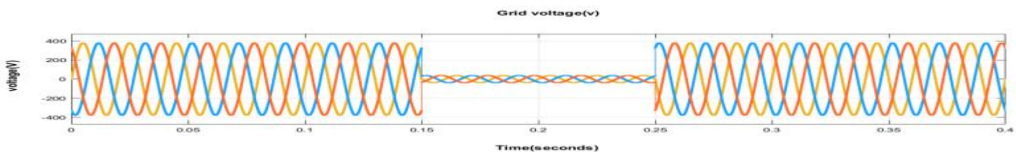

(a)

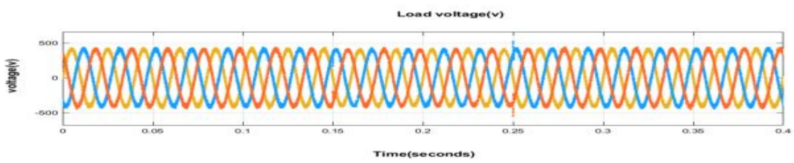

(b)

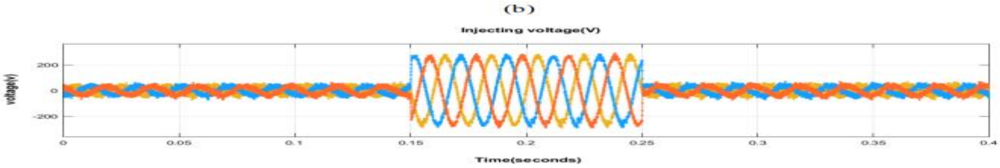

(c)

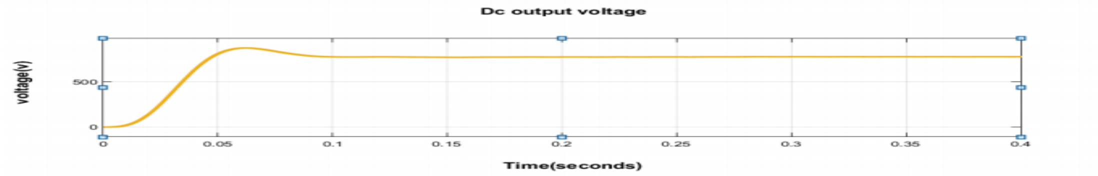

(d)

Fig. 17. Performance characteristics with FRTC at 90% sag.

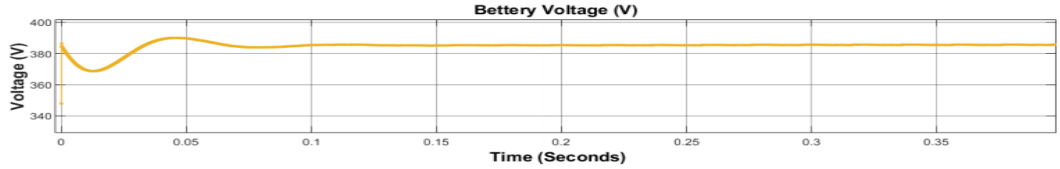

(b)

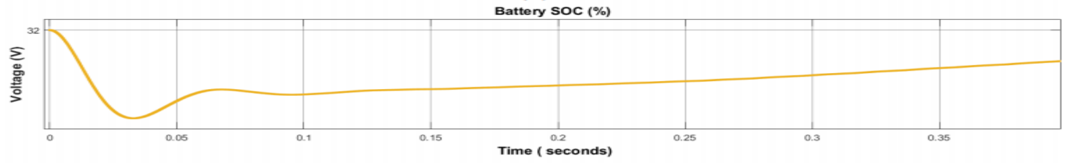

(c)

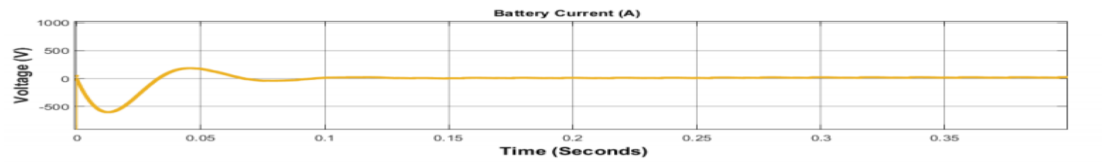

(a)

Fig. 18. Battery characteristics with FRTC at 90% sag.

V. Conclusion

The effects of different voltage sag levels on the EV charging system and batteries were investigated in the present research, which also introduced the DVR-FRTC system to enhance the load voltage quality. The MATLAB/Simulink platform is used to simulate the system in order to conduct the simulation analysis. The dSPACE (DS1202) real-time system's SIL test is used for the real-time validation. The performance of the system is assessed at 30%, 60%, and 90% voltage sag levels both with and without the DVR-FRTC system. When there is a 30% voltage drop, the charging system without DVR-FRTC is in the stable mode; when there is a 60% and 90% voltage drop, it remained in the unstable mode. Due to the DVR-FRTC system ability to inject voltage during the sag period and maintain the load voltage at a standard value, the charging system with this technology operated in the stable mode for all voltage sag levels. Consequently, the system is operating in the stable mode all the time. In addition to increasing system dependability, it protects the EV batteries from voltage fluctuations. Analysis of the health effects of the battery and converter components with and without the DVR-FRTC system can be part of this study.

REFERENCES

[1] H.S. Das, M.M. Rahman, S. Li, and C.W. Tan, “Electric vehicles standards, charging infrastructure, and impact on grid integration: A technological review,” Renew. Sustain. Energy Rev., vol. 120, Mar. 2020, Art. no. 109618.

[2] M.R. Khalid, M.S. Alam, A. Sarwar, and M.S. J. Asghar, “Acom prehensive review on electric vehicles charging infrastructures and their impacts on power-quality of the utility grid,” e Transportation, vol. 1, Aug. 2019, Art. no. 100006.

[3] M. H. J. Bollen, Solving Power Quality Problems: Voltage Sags and Interruptions. New York, NY, USA: IEEE Press, 1999, p. 139.

[4] W. E. Kazibwe and M. H. Sendaula, Electric Power Quality Control Techniques. New York, NY, USA: Van Nostrand Reinhold, 1993, p. 11.

[5] J. Xiong, K. Zhang, Y. Guo, and W. Su, “Investigate the impacts of PEV charging facilities on integrated electric distribution system and electrified transportation system,” IEEE Trans. Transport. Electrific., vol. 1, no. 2, pp. 178–187, Aug. 2015.
[6] S. Rahman, I. A. Khan, A. A. Khan, A. Mallik, and M. F. Nadeem, “Comprehensive review & impact analysis of integrating projected electric vehicle charging load to the existing low voltage distribution system,” Renew. Sustain. Energy Rev., vol. 153, Jan. 2022, Art. no. 111756.
[7] S. Habib, M. M. Khan, F. Abbas, L. Sang, M. U. Shahid, and H. Tang, “A comprehensive study of implemented international standards, technical challenges, impacts and prospects for electric vehicles,” IEEE Access, vol. 6, pp. 13866–13890, 2018.
[8] Y. O. Assolami, A. Gaouda, and R. El-Shatshat, “Impact on voltage quality and transformer aging of residential prosumer ownership of plugin electric vehicles: Assessment and solutions,” IEEE Trans. Transport. Electrific., early access, Jun. 15, 2021, doi: 10.1109/TTE.2021.3089460.
[9] Power Quality Requirements for Plug-In Electric Vehicle Chargers, Standard J2894-1, Society of Automotive Engineers, Dec. 2011.
[10] Z. Wang, X. Guo, J. Li, and X. Wang, “Impact of voltage sags on electric-vehicle charger and critical voltage sag determination,” IEEE Trans. Power Del., vol. 31, no. 3, pp. 1397–1399, Jun. 2016.
[11] X. Guo, J. Li, and X. Wang, “Impact of grid and load disturbances on electric vehicle battery in G2V/V2G and V2H mode,” in Proc. IEEE Energy Convers. Congr. Expo., Montreal, QC, Canada, Sep. 2015, pp. 5406–5410.
[12] S. Hui and X. Yonghai, “Study on the impact of voltage sags on different types of electric vehicle chargers,” in Proc. China Int. Conf. Electr. Distrib. (CICED), Xi’an, China, Aug. 2016, pp. 1–4.
[13] C. Zhou, K. Qian, M. Allan, and W. Zhou, “Modeling of the cost of EV battery wear due to V2G application in power systems,” IEEE Trans. Energy Convers., vol. 26, no. 4, pp. 1041–1050, Dec. 2011.
[14] C. Tu, Q. Guo, F. Jiang, H. Wang, and Z. Shuai, “A comprehensive study to mitigate voltage sags and phase jumps using a dynamic voltage restorer,” IEEE J. Emerg. Sel. Topics Power Electron., vol. 8, no. 2, pp. 1490–1502, Jun. 2020.
[15] A. Khergade, R. Satputaley, and S. K. Patro, “Investigation of voltage sags effects on ASD and mitigation using ESRF theory-based DVR,” IEEE Trans. Power Del., vol. 36, no. 6, pp. 3752–3764, Dec. 2021.
